Adaptive flow control laws: A simulation based comparison with low order models

C. Raibaudo* Ph. Mouyon† C. Döll‡

ONERA - DTIS, Toulouse, 31055, France

Contents

*Post-Doctorant, ONERA-DTIS, 2, avenue Edouard Belin, 31055 Toulouse Cedex 4, France.
†Expert, ONERA-DTIS, 2, avenue Edouard Belin, 31055 Toulouse Cedex 4, France.
‡Senior Specialist, ONERA-DTIS, 2, avenue Edouard Belin, 31055 Toulouse Cedex 4, France.

1. Introduction

In the past few decades, the control of turbulent boundary layers separation has been crucial for aerodynamic performances improvement [1]. Passive devices, like vortex generators, have been first considered for an efficient redistribution of the energy between the external fluid and the separation region [2]. The separation process is yet sensitive to unsteady upstream perturbations and related to the absolute instability of the flow [3]. Active flow control (AFC) is therefore preferred and offers more flexibility in the control parameters. An adaptation of the airfoil shape to the speed or the weight could also increase the performances during the flight. For this objective, a multi-disciplinary research platform involving European partners has been created for the development of an electro-active morphing wing. Both low-frequency camber control and high frequency vibrating trailing edge (HFVTE) serve as actuators for the wing. The HFVTE in particular will be used for the feedback control. The actuator vibration is about the millimeter in amplitude and up to 200 Hz in frequency. Pressure taps are also located upstream to the leading edge on the upper surface. Two 6 mm diameter microphones and one dynamic pressure sensor (Kulite XCQ063) are put to measure the characteristic state of the flow under control in real-time. More details on the actuators and preliminary open-loop results can be found in [4] and [5].

In order to increase the robustness and maintain performances despite disturbances and uncertainties, active flow control should be performed in closed-loop control. The design of a closed control law is generally based on a system model of rather low order. This model must keep the main characteristics of the flow, with its control input and output. High non-linear behavior of flows, disturbances and uncertainties on the model (on speed, pressure, temperature, Reynolds number...) make model-based control more difficult to achieve [6]. Adaptive methods are therefore useful techniques to deal with these unmodeled effects. Extremum-seeking [6, 7] and slope-seeking [8, 9] have been used in the past for flow control applications, but more progress could be achieved in this field. Different techniques can be considered: (i) a model free approach using polynomial approximation of the dynamics [10], (ii) direct adaptive control consisting on tuning the gains on-line of a feedback loop in order to minimize a given criterion [11] and (iii) indirect adaptive control consisting on estimate on-line a system model and use it to design the control law [12]. The present study will focus on the analysis of the natural flow dynamics of the experimental morphing wing in order to obtain low order dynamical models, as attractors, and the development of direct adaptive techniques for the stabilization of the flow in closed-loop control.

Figure 1 shows the main ingredients of the simulation developed. Two reduced order models of the flow are suggested. The first one is the classical nonlinear Van der Pol oscillator. The second one is the previous Van der Pol oscillator with the pulsation perturbed by random signal. This yields to a more realistic representation of the measurement signal, with a broadband spectrum.

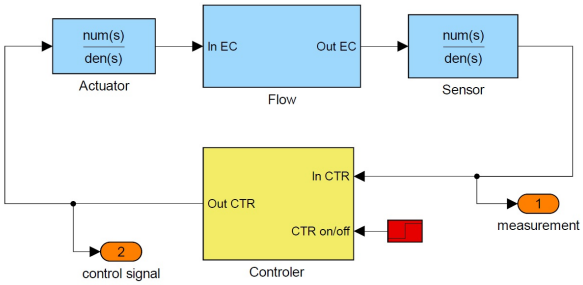

Figure 1: Block diagram for the flow control.

Using these models, several controllers are developed and compared their performances. We first highlight the limitation of the simple control laws conventionally used to suppress the oscillations of Van der Pol models. An advantage of these laws is that it is relatively easy to adapt them in real time. We describe and test many of these adaptation procedures. Then we introduce more sophisticated control laws (dynamic and not static controllers). The adaptation of these command laws is however more touchy. Some ways to implement the controller are to be favoured to facilitate its adaptation and avoid the occurrence of instability flares. This is already known in adaptive filtering of signals, but amplified here by the fact of working in closed loop. Finally, an architecture with a double adaptation is proposed. It makes it possible to regulate the power of the injected control signal on the one hand, and on the other hand to adjust the dynamic behavior.

2. Approximated model of the flow for the law design

Fluids usually consist of multiple-frequency dynamics. For the configuration considered, significant frequencies have been found in the previous studies in the PSD of temporal coefficients modes of the POD corresponding to different physical phenomena in the airfoil wake [5]. The complexity of the flow dynamics will be confirmed in the next section. In order to design closed loop control laws we use a model that approximated the behavior of the flow along with its actuators and sensors. The model must not be too much complex so that it can be used easily for control design purpose. Nevertheless it must capture the main characteristics of the phenomenon to be control. In the present case the control is intended to reduce intrinsic vibratory phenomenons that are present in the flow model. A careful consideration of the flow frequencies in this low-order model used for the simulation is then crucial. Nonlinear oscillators such as the Van der Pol (VdP) oscillator are therefore an satisfying choice. Van der Pol non-linear oscillator is chosen from previous works as being able to represent flow stability and dynamics [13]. This model has been used to reproduce and control the dynamics of simplified bluff bodies [14] or airfoils [15] for example.

The difficulty we encountered in order to work in 3D complex flows comes in part from the fact that the spectrum of the measures in 3D is broadband and no longer narrow band as in 2D. In order to model such a behavior we introduce a nonlinear chaotic oscillator that is known to deliver a broadband signal still in an intrinsic fashion. Coupling the two oscillators yields to a more realistic model of the flow to be control. Pressure dynamics on the experimental airfoil will be acquired to design low-order VdP models with corresponding frequencies of oscillation.

2.1. Quasi-harmonic nonlinear oscillator

The state space representation for the controlled Van der Pol model is expressed as:

$$\left\{ \begin{array}{lcl} \dot{x}_1 & = & x_2 + G\,u \\ \dot{x}_2 & = & -\omega_0^2 x_1 + \left(2\xi\omega_0 - 3K_s x_1^2\right)\,(x_2 + G\,u) \\ y & = & x_1 \end{array} \right. \tag{1}$$

where x_1, x_2 are the states of the system, y is the measured output, and u is the control input.

System (1) can be rewritten as a second order ordinary differential equation:

$$\ddot{y} - 2\,\xi\,\omega_0\,\dot{y} + 3\,K_s\,y^2\,\dot{y} = G\,u \tag{2}$$

The determination of the constants is realized using the permanent regime response. More details can be found in [13].

Figure 2 shows the time history and Power Density Spectrum (PSD) of the response of the unforced VdP model. The interest of the VdP oscillator is the self-sustained oscillations are maintained even when the actuation is off. This corresponds to physical phenomenons in fluid mechanics such as the vortex shedding dynamics behind a bluff body or an airfoil.

2.2. Enlargement of the oscillator spectral properties

Enlargement of the spectrum band around the main pulsation ω_0 of the oscillator is now considered in figure 3 through a spectral analysis. The PSD is computed from the post-filtered pressure signal s for each sensor using the Welch's method:

$$PSD_s(f) = \sum_{m=-\infty}^{\infty} E\{s_{n+m}s_n^*\}\; e^{-j2\pi fm} \tag{3}$$

Modulation of the phase is achieved by random fluctuations of the pulsation $\omega = \omega_0 + \omega_{rand}$. The size of the enlargement is approximated with the experimental data presented in the next section.

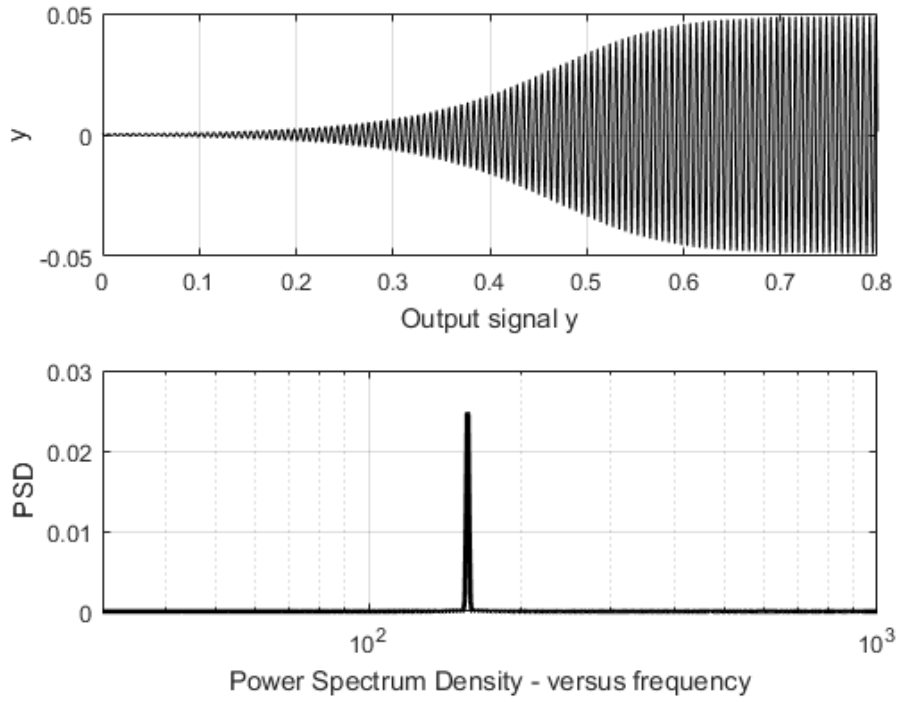

Figure 2: Time history and PSD of the unforced response with self-sustained oscillations (from [13]).

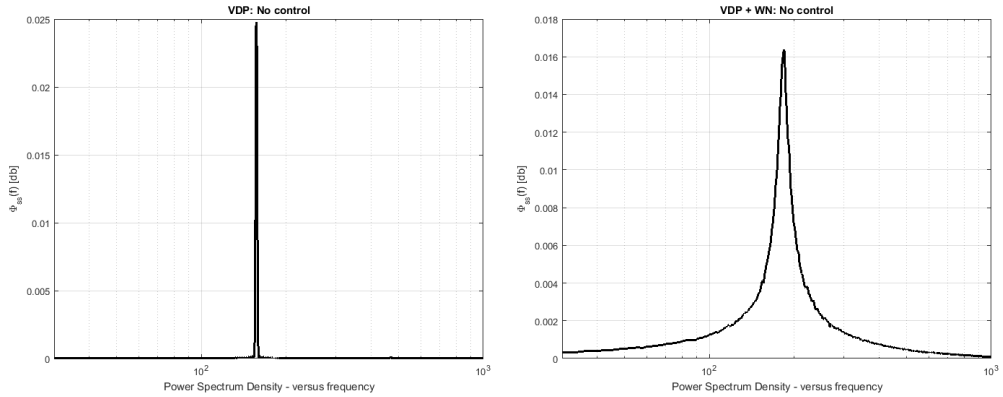

Figure 3: Spectrum of the system output without control. (a) Without and (b) with fluctuations around the main frequency.

3. Identification of the model using experimental set-up

The experimental set-up is presented here. Experimental data of the steady flow without control (noted baseflow) is acquired for this study to design a realistic representation of the flow dynamics.

3.1. Experimental set-up

The experimental system to control is a A380 morphing wing at a reduced scale in order to optimally modify the aircraft shape and increase performances of the wings [5]. The chord is $c = 0.7$ m and the span length 0.59 m. Coordinates on the wing are noted x and y, respectively in the streamwise and spanwise directions from the leading edge. The wing wake is controlled by Higher Frequency Vibrating Trailing Edge (HFVTE) actuators, using piezoelectrical components. The HFVTE are able to reach frequencies of actuation up to 450 Hz and amplitudes of about the millimeter. More details of the system in [5].

The wing model is tested in the subsonic wind tunnel of the Institut de Mécanique des Fluides de Toulouse (IMFT). Tests are performed at free stream velocities $U_\infty = 10.6$ and 21.5 m/s, for turbulence intensity of about 0.1 %. The resulting Reynolds numbers are respectively 5.10^5 and 10^6.

Pressure sensors are put on the extrados of the wing to measure the flow dynamics without and with actuation. Sensors are set at the same spanwise position $y_1/c = y_2/c = 0.56$, but different streamwise locations: $x_1/c = 0.6$ and $x_2/c = 0.8$. To measure frequencies of the order of 100 Hz, the sample frequency is set at $F_s = 16.7$ kHz and the anti-aliasing filter frequency at 8.4 kHz. Time of acquisition is $T_a = 60$ s, corresponding to about 9000 cycles of the expected frequency of the flow.

3.2. Dynamics of the natural flow

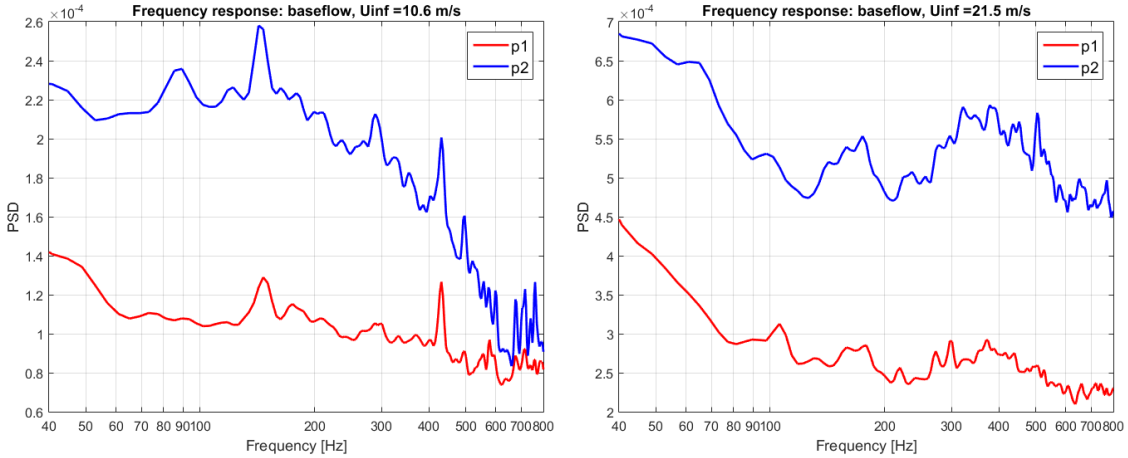

Figure 4: Spectrum of the baseflow with $U_\infty =$ (a) 10.6 m/s and (b) 21.5 m/s, for sensors at $x/c = 0.6$ (red) and 0.8 (blue).

The natural flow dynamics is characterized in figure 4 by the PSD of the pressure signal is computed similarly simarly as the simulated system and expressed by Eq. 3. For $U_\infty = 10.6$ m/s, main frequencies between 150 and 200 Hz, and their harmonics, are observed and corresponds to the dynamics found in previous studies [5]. The nature of the flow dynamics shows a larger spectrum band and not only a single line. The use of complex models for the flow is therefore justified. Our control objective is to reduce the PSD within this frequency range [150,200] Hz.

4. Adaptive control law structures

Several adaptations strategies have been considered in this study. A general architecture would be composed of four blocks (see figure 5).

- A first block is used on practical expriments in order to formate the aerodynamic measurements delivered by the sensors into the signal y. It may consist in a simple scaling, but could be far more complex depending on the physics of the sensing process.
- A second block evaluates a performance criterion J calculated from the measurements. A nonlinear filter is usually used to estimate the instantaneous standard deviation of the acquired signals.
- A thrid block optimizes the parameters of the control law in order to minimize this criterion.
- And a last bloc is the computation of the control signal u itself that will be fed to the actuator.

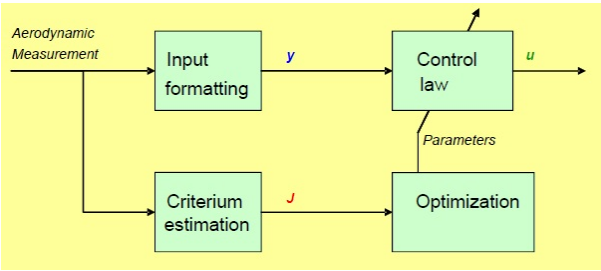

Figure 5: The overall control architecture

4.1. Static gain controller with delayed measurement

Static gain controller is first considered. It corresponds by fixing the gain and delay manually of the output feedback control

$$u(t) = K\ y(t - \tau) \tag{4}$$

This controller is known to be able to suppress oscillations of Van der Pol models. Indeed, a Van der Pol oscillator is a linear unstable dynamical system, along with a non linear feedback that prevents the divergence when the amplitude of the oscillations becomes too great. Thus any linear feedback stabilizing the linear dynamic will remove the limit cycle. As the characteristics of the Van der Pol model are not well known, finding the value of the feedback gain K that suppresses the oscillations is difficult. An online adaptation of the gain K is therefore used for that purpose, as well as the delay τ, to first estimate their value. An optimum around $K = 90$ (for the unpertubed VdP), $K = 125$ (for the perturbed VdP), and $\tau = 10.T_s$ (T_s the simulation step precised in 5.1) has been found and is used here.

4.2. Adaptation of the gain

The gain in particular can be optimized online using adaptive methods. Several adaptations procedures have been developed to optimize the parameters of the control law (here the gain K) in order to minimize a criterion $\mathcal{J}_n$, based on the standard deviation of the signal y, as:

$$\mathcal{J}_n = \sum_{j=j_c}^{n} y_j^2 \tag{5}$$

with j_c the index of the control start. The total cost function corresponding to the full simulation is noted $\mathcal{J}$. The present study will focus on few methods to obtain the gain minimizing the cost function.

4.2.1. Gradient descent

The optimal gain K^* is iteratively found by a gradient descent of K as:

$$K = K^* - \mu_K \frac{d\mathcal{J}}{dK} \tag{6}$$

with μ_K the adaption step. μ_K is adapted at each actualization using the derivative and the optimal cost function $\mathcal{J}^*$

$$\mu_K = \alpha_\mu \ \mathcal{J}^* \ / \ \left(\frac{d\mathcal{J}}{dK}\right)^2 \tag{7}$$

At first order, the criterium should evolve according to $J = (1 - \alpha_\mu) \ \mathcal{J}^*$. Thus α_μ is set to the expected relative rate of the criterium.

4.2.2. Local grid optimization

The gain optimization can also be carried out by exploration of a local grid of gains is generated for each iteration around K^*. The optimization process reduces to the choice of the tuning minimizing the criterium with this grid. To acheive good performances, the grid must adapted online. Its extend is reduced as criterion converges.

4.3. Delay controller

The complementary procedure of the previous method is to implement a static feedback applied to the delayed measurement (Eq. 4) and tune the delay τ by keeping the gain constant. After the previous optimal gains are obtained ($K = 90$ and 120), the delay τ is scanned from 0 to $1/f_{nat} = 33.T_s$, the maximal value possible on a periode.

4.4. Dynamic controller in rational form

The controller structure is a linear dynamical system described by its transfer function:

$$K(s) = \frac{N(s)}{D(s)}$$

where N and D are polynomial functions using the Laplace variable s. In practice this controller is often implemented as an ARMA filter (and sometimes in a state space form). The parameters of the control law are the coefficients of the polynomials N and D. Such a control structure is very difficult to adapt online while acheiving closed loop stability. Indeed, the controller becomes instable when the measurement y is stabilized because there is not enougth information in the signal and the adaptation is only driven by the noise. As soon as the controller became unstable, the system natural oscillations reappears. And the controller converges again.

4.5. Dynamic controller in lattice form

Lattice form is another way to implement linear dynamic filters. The general structure of the filter (from [16]) is presented in figure 6. Regalia [17] has proposed several efficient tools to adapt such filters while preserving stability of the filter. Here we use these tools to adapt a controller in a feedback loop. Some attention must be paid to avoid some unexpected behaviors. These results in a two stage adaption procedure. One stage adapts the static gain of the controller. The other stage dapts the dynamical part of the controller. Different orders of the lattice filters have been tested. $N_{lattice} = 20$ is here presented. For the adaptation of the gain, the same parameters are used for this method as previously.

5. Simulation results

Results of the simulation with the previous feedback controllers are presented in this section. Both unperturbed and frequency perturbed Van der Pol oscillators are considered. In particular, the effect of a large band spectrum on the control will be observed. In the present section, the time histories of the system output $y(t)$ and the control $u(t)$ will be presented respectively on top and bottom of all figures.

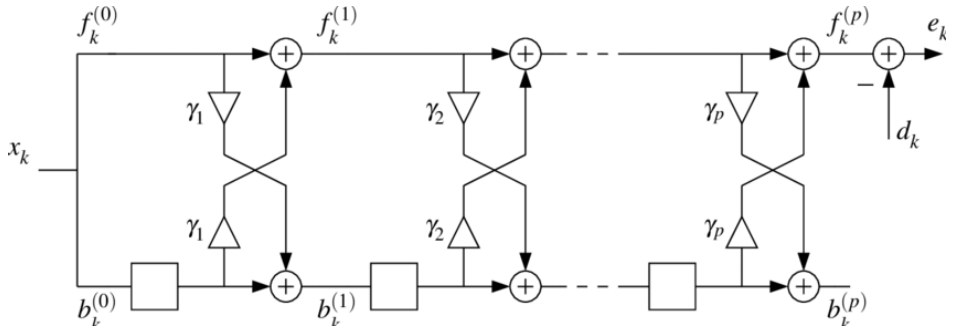

Figure 6: Structure of the adaptive lattice filter (from [16])

5.1. Simulation parameters

All the cases are simulated using Matlab/Simulink. The time step for the simulation is $T_s = 0.0002$ s, and the actuation is actualized every $10T_s$. The oscillator without control is firstly simulated, and is fully stable when the control is applied at $T_c = 10$ s. The total simulation is 180 s. The actuation signal u is saturated to stay positive, and the control gains remains between ± 200.

5.2. Control of the unperturbed Van der Pol oscillator

Results of the unperturbed oscillator are summarized in figure 7. For the static controller, two scan tests are shown: one for the gain, the other for the delay. From these scans, optimal value may be deduced and then are used in a fluid test. Whatever the adaptation method considered, the feedback controller succeeds to reduce the instantaneous standard deviation of the signal y. For the scan of gain (Fig. 7 (b)), the method found optimal gains that stabilizes the system. But as the scan continues between the specified range, successions of stabilization and destabilization of the system are observed. For all the methods, complete stabilization is achieved after 20 secondes of actuation.

5.3. Control of the perturbed Van der Pol oscillator

A more complex dynamics make the system more difficult to control. Results of the pulsation-perturbed oscillator are summarized in figure 8. Similarlly to the system without perturbation, varying the gain by scan (Fig. 8(b)) periodically stabilizes and destabilizes the system. The fixed gain and delay (Fig. 8(a)), the optimization of the gain by gradient (Fig. 8(c)), and the scan of delay (Fig. 8(e)), shows a global improvement of the signal reduction, but not a complete stabilization. The adaptation of the lattice form and gain (Fig. 8(f)) is therefore more efficient for the system stabilization and the control speed.

The position of the zeros and poles for the lattice filter during the adaptive last procedure is shown in figure 9. With a pure VdP system (a), zeros are distributed on the unit circle to cancel the quasi-harmonic oscillator. A larger dispersion of the poles and the zeros is observed with the perturbed Van der Pol (b), but stay inside the unit circle. However, it does not impact the capability of the control of reorganize the zeros and the poles.

6. Concluding remarks

Closed-loop feedback control was considered for the stabilization of a morphing wing flow by trailing edge vibration. A direct adaptive control is applied to a low-order dynamical oscillator. A Van der Pol nonlinear oscillator coupled with a fluctuation of the pulsation is used as a representative model of the flow. Simulations tests show significant results obtained using a lattice filter and an adaptive gain. A complete stabilization of the output was performed with little information needed of the system.

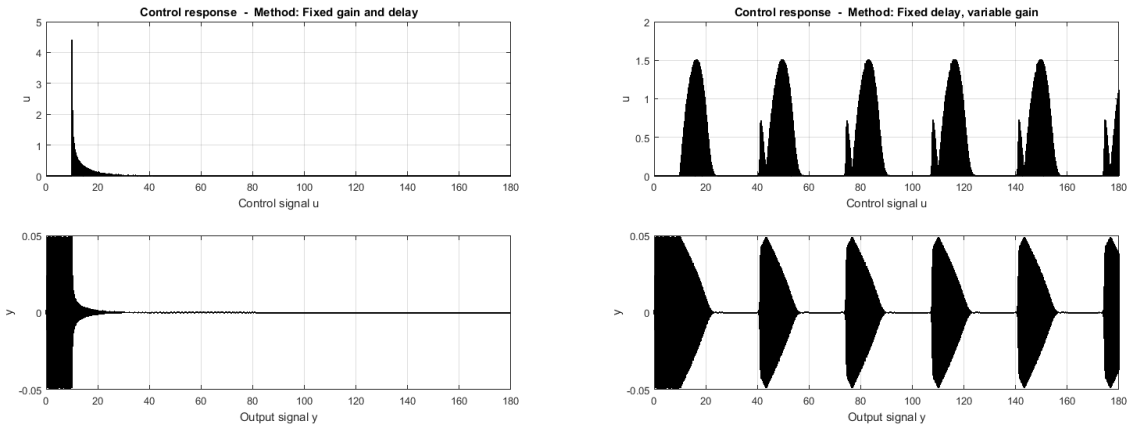

(a)

(b)

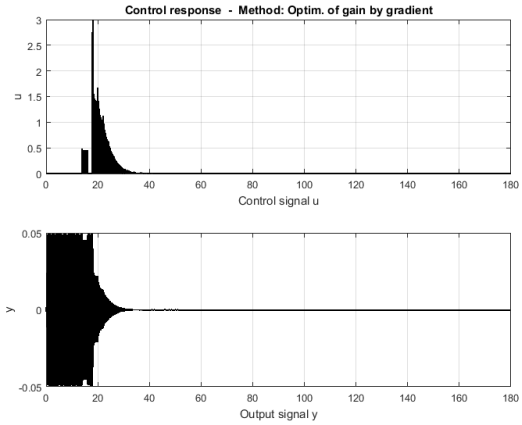

(c)

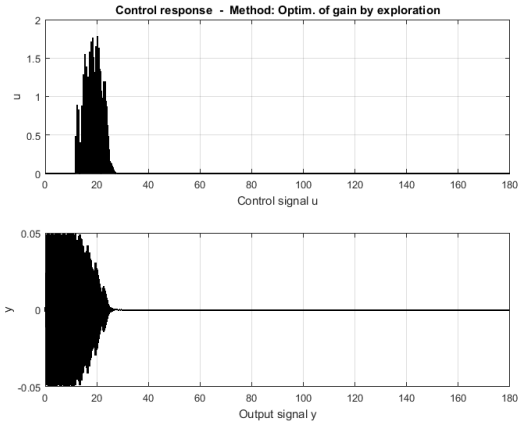

(d)

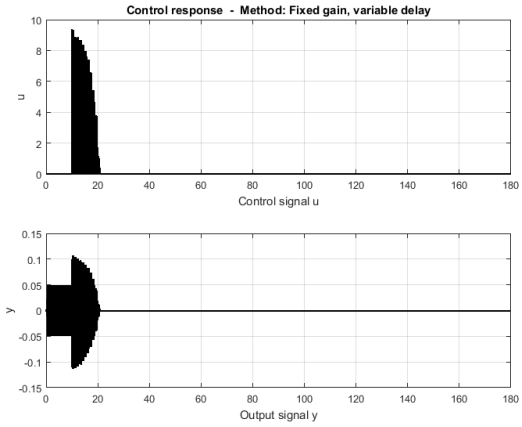

(e)

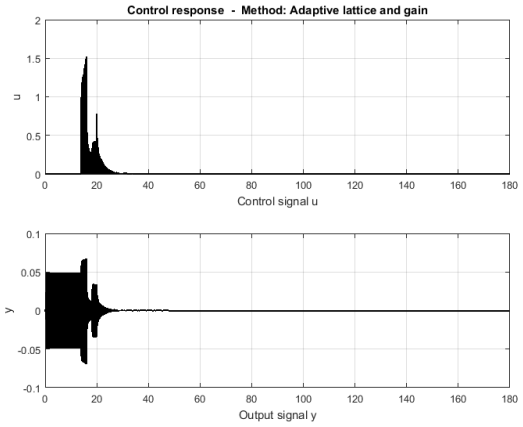

(f)

Figure 7: Results of the closed-loop control of the unperturbed Van der Pol with different control stratagie. Methods: (a) Fixed gain and delay, (b) fixed delay and scan on gain, (c) optimization of the gain by gradient, (d) optimization of the gain by exploration, (e) fixed gain and scan on delay and (f) adaptive gain and lattice filter.

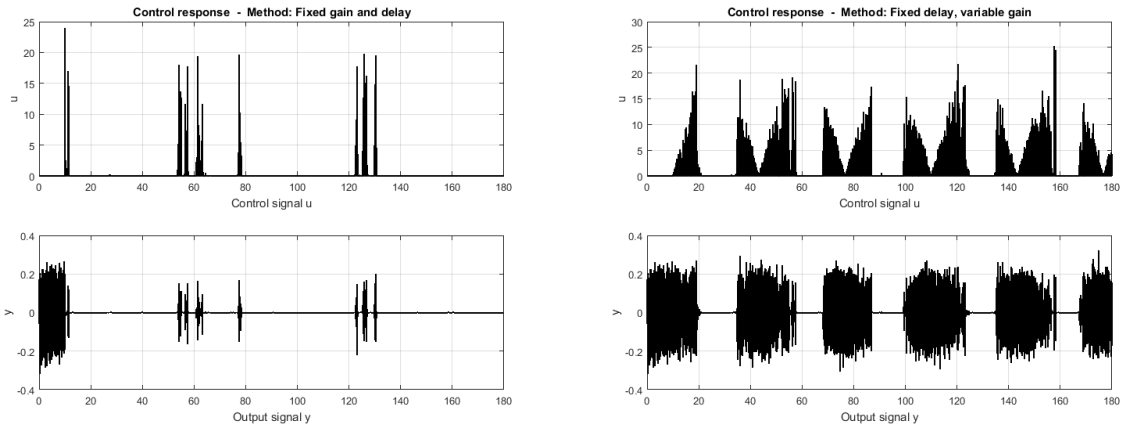

(a)

(b)

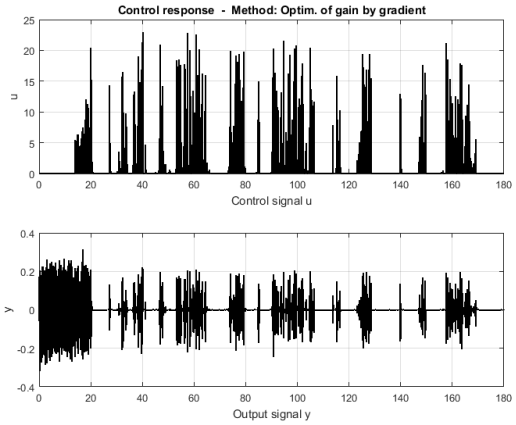

(c)

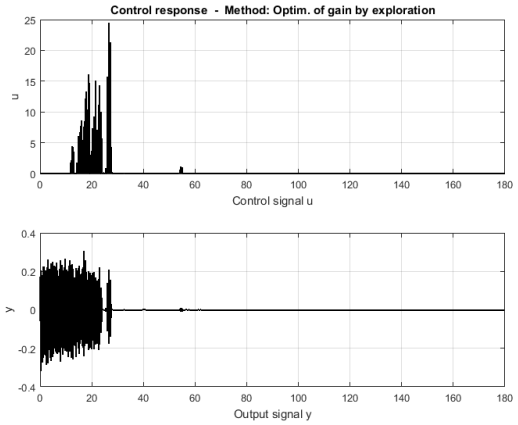

(d)

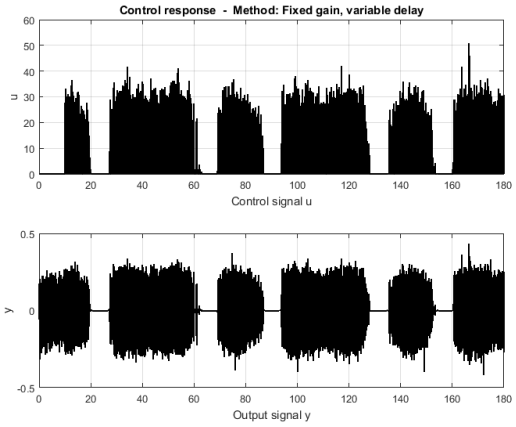

(e)

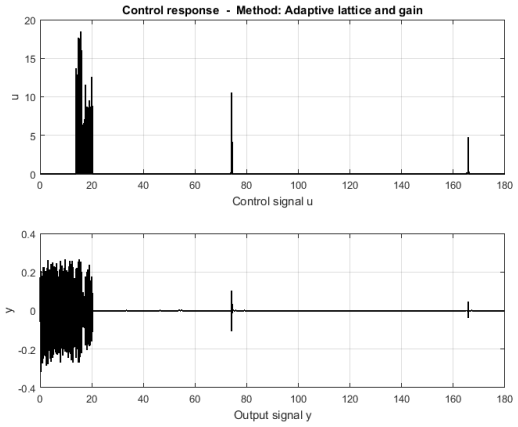

(f)

Figure 8: Results of the closed-loop control of the perturbed Van der Pol with different control stratagie. Methods: (a) Fixed gain and delay, (b) fixed delay and scan on gain, (c) optimization of the gain by gradient, (d) optimization of the gain by exploration, (e) fixed gain and scan on delay and (f) adaptive gain and lattice filter.

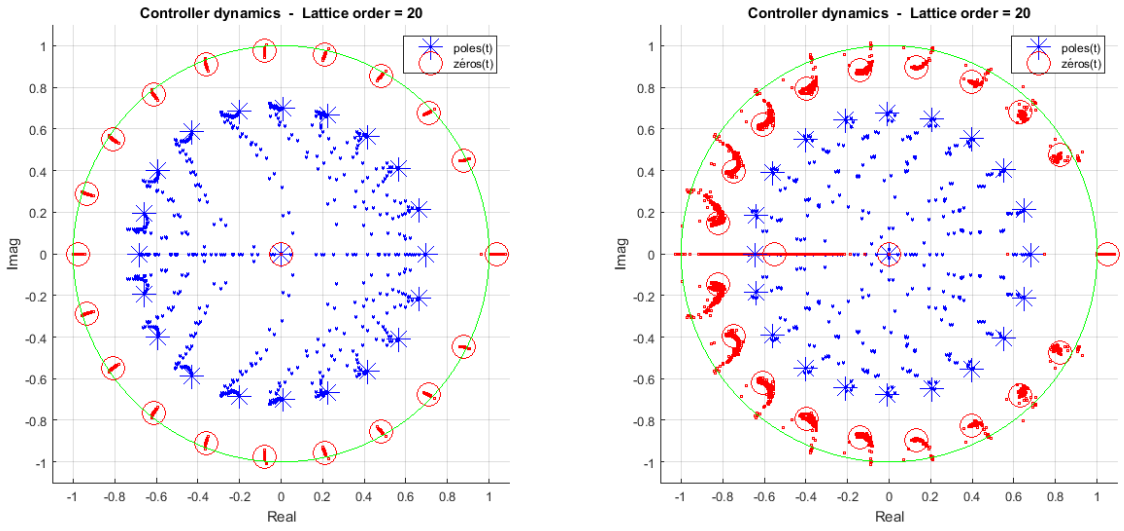

(a) (b)

Figure 9: Position of the zeros and poles of the lattice filter after the adaptive gain and lattice procedure with (a) unperturbed VdP and (b) perturbed VdP.

Acknowledgments

This work is supported by the European project H2020 Smart Morphing and Sensing SMS (http://www.smartwing.org/SMS/). The authors thank Mateus Carvalho and Dr. Marianna Braza for the acquisition and the analysis of the experimental data.

References

[1] Gad-el hak, M. Turbulence Control and Applications. Tutorial School on Fluid Dynamics : Topics in Turbulence. College Park, Maryland, USA, 2010.

[2] Lin, J. C. Review of research on low-profile vortex generators to control boundary-layer separation. *Progress in Aerospace Sciences* **2002**, *38*, 389–420.

[3] Marquillie, M.; Ehrenstein, U.; Laval, J.-P. Instability of streaks in wall turbulence with adverse pressure gradient. *Journal of Fluid Mechanics* **2011**, *681*, 205–240.

[4] Scheller, J.; Jodin, G.; Rizzo, K. J.; Duhayon, E.; Rouchon, J. F.; Triantafyllou, M.; Braza, M. A Combined Smart-Materials Approach for Next-Generation Airfoils. *Solid State Phenomena* **2016**, *251*, 106–112.

[5] Jodin, G.; Motta, V.; Scheller, J.; Duhayon, E.; Döll, C.; Rouchon, J. F.; Braza, M. Dynamics of a hybrid morphing wing with active open loop vibrating trailing edge by time-resolved PIV and force measures. *Journal of Fluids and Structures* **2017**, *74*, 263–290.

[6] Garwon, M.; Darmadi, L.; Urzynicok, F.; Bärwolff, G.; King, R. Adaptive control of separated flows. Proc. of the ECC. Cambridge, United Kingdom, 2003.

[7] Tian, Y.; Cattafesta, L. N.; Mittal, R. Adaptive Control of Separated Flow. 44th AIAA Aerospace Sciences Meeting and Exhibit. Reno, Nevada, USA, 2006.

[8] King, R.; Becker, R.; Feuerbach, G.; Henning, L.; Petz, R.; Nitsehe, W.; Lemke, O.; Neise, W. Adaptive flow control using slope seeking. 14th Mediterranean Conference on Control and Automation. Ancona, Italy, 2006.

[9] Henning, L.; Becker, R.; Feuerbach, G.; Muminovic, R.; King, R.; Brunn, A.; Nitsche, W. Extensions of adaptive slope-seeking for active flow control. *Proceedings of the Institution of Mechanical Engineers. Part I: Journal of Systems and Control Engineering* **2008**, *222*, 309–322.

[10] Fliess, M.; Sira-Ramírez, H. Closed-loop parametric identification for continuous-time linear systems via new algebraic techniques. *Advances in Industrial Control* **2008**, 363–391.

[11] Widrow, B.; Lehr, M.; Beaufays, F.; Wan, E.; Bilello, M. Adaptive signal processing. 1993.

[12] Kreisselmeier, G. An approach to stable indirect adaptive control. *Automatica* **1985**, *21*, 425–431.

[13] Motta, V.; Mouyon, P.; Döll, C. Discrete Time Open-Loop and Closed-Loop Flow Control Based on Van der Pol Modeling. 8th AIAA Flow Control Conference. Reston, Virginia, 2016.

[14] Provensale, M.; Mathis, C.; Boyer, L. Benard-von Karman instability: Transient and forced regimes. *Journal of Fluid Mechanics* **1987**, *182*, 1–22.

[15] Khalid, M. S. U.; Akhtar, I. Modeling the Aerodynamic Lift Produced by Oscillating Airfoils at Low Reynolds Number. **2014**, 1–23.

[16] Flanagan, M. F.; McLaughlin, M.; D.Fagan, A. Gradient-adaptive algorithms for minimum phase-all pass decomposition of an FIR system. *IET Signal Processing*

[17] Regalia, P. A. An Improved Lattice-Based Adaptive Iir Notch Filter. *IEEE Transactions on Signal Processing* **1991**, *39*, 2124–2128.